Current Natural Sciences & Engineering
Volume 3, Issue 1, 2026, 928-945

Optimization of Lead-Free $CsSnCl_3$ Perovskite Solar Cells by Electron and Hole Transport Layer Property Modulation Utilizing SCAPS-1D

Yashika Agarwal[1], Saanvi Suri[1], Adit Kumar[1] and Nitish Saini[1*]

[1] *DPS International, Golf Course Extension Road, Sector 50, Gurgaon, 122018, India.*

Received date:14/04/2026, Acceptance date: 18/05/2026

DOI: ***http://doi.org/10.63015/1her-2502.3.1***

Corresponding author: *nitish2593@gmail.com*

Abstract

Photovoltaics are key to the realization of the United Nations Sustainable Development Goals, with over 60 percent of global electricity projected to be supplied by solar energy by 2050, however, traditional silicon solar cells have been associated with high cost of fabrication, energy content and the electronic waste. Although high-performing, with their ABX_3 crystal structure that allows them to absorb strongly, transfer charges efficiently, and tune their bandgaps, lead-based perovskite solar cells (PSCs) are toxic and lacks stability issues that limit their application on the parameter of sustainability. This prompts the design of lead-free perovskites, among which cesium tin chloride ($CsSnCl_3$) is non-toxic, has an appropriate bandgap (1.3 -1.8 eV, depending on the conditions of modelling the material and its defects), and better ambient stability. It is observed that the perovskites based on chloride tend to have larger intrinsic bandgaps (>2 eV), thus, the effective bandgap used in this paper represents parameters that were actually simulated and not necessarily actual experimental results. Using SCAPS-1D, an all-inorganic CBTS/$CsSnCl_3$/ZnO heterostructure is optimized. The power conversion efficiency of 16.95% was achieved due to optimization. Theoretical simulations predict efficiency under ideal conditions, however, practical values are often lower due to defects, interface losses, and fabrication constraints.

Keywords: Perovskite Solar Cell (PSC), Hole Transport Layer (HTL), Electron Transport Layer (ETL), Lead-free Perovskites, Power Conversion Efficiency (PCE).

1.Introduction

In the context of increasing world energy consumption, exhaustion of fossil fuels, and the ever-growing fear of carbon emission and climate change, the creation of renewable energy technologies has become more and more essential [1]. Among these, solar energy is unique in terms of its quantity and the ability to scale. Perovskite solar cells (PSCs) have been particularly of interest in this respect due to their remarkable optoelectronic characteristics, such as high absorption coefficients, tunable bandgaps, long carrier diffusion lengths, and high carrier mobility [2]. These strengths make the PSCs as promising alternatives to the existing silicon based technologies that are facing problems in costs and environmental effects. The perovskites include a very broad variety of materials, including organic-inorganic hybrids and totally inorganic compounds. Although efficiencies of hybrid perovskites can be very high, they tend to be affected by the problem of stability, in contrast to the case of inorganic variants of perovskite, e.g. Cs-based halides, where thermal and structural stability is generally much higher [3]. The direct bandgap of perovskite materials allows efficient photon absorption and electron–hole pair generation without phonon assistance, thereby reducing recombination losses and improving charge extraction [4]. Lead based perovskite solar cells are highly efficient, due to their excellent optical and electronic properties, with the PCE of these lead based cells increasing from a mere 3.8% to 25.8%. [5]. However, the toxicity of lead (Pb) poses an encumbrance for large scale production and implementation of solar technology due to its environmental concerns and impact on human health. [6]. Consequently, current literature has devoted efforts to discovering alternative materials for similar applications. Metal halide perovskites - commonly based on elements like tin (Sn), germanium (Ge), and bismuth (Bi) - are environmentally friendly materials as they consist of entirely inorganic components which allow for reduction in costs and toxicity. [7,8].

Of these, Sn-based perovskites are frequently studied due to their favourable optoelectronic characteristics and enhanced stability. Tin can be found in various oxidation states and structural phases, which affects the material performance. Specifically, $CsSnCl_3$ presents a viable alternative for lead based solar cells owing to its high absorption coefficient (α), favourable carrier mobility, and suitable bandgap for effective high efficiency solar cell applications. [9]. PSCs performance highly relies on device architecture and charge transport layers. Electron transport layers (ETLs), hole transport layers (HTLs) are important in terms of charge extraction, recombination suppression and energy level alignment [10]. PSCs are generally designed in n-i-p or p-i-n devices, with the n-i-p device providing flexibility to systematic optimisation of transport layers and device parameters [11]. Although $CsSnCl_3$ based PSCs hold promise, the research is still immature in comparison to lead-based systems like $FAPbI_3$ and $MAPbI_3$, leaving key performance mechanisms poorly understood [12]. The isolation of effects of interdependent parameters is often challenged by experimental approaches and this has led to the use of numerical simulation to systematically optimise device properties.

We use numerical simulations in this research to explore $CsSnCl_3$ based PSCs and determine the best heterostructure designs. Our analysis is aimed at maximising the performance of the device in terms of PCE, open-circuit voltage (VOC), short-circuit current density (JSC), and fill factor. Our results provide important design criteria, such as an optimal absorber thickness (~0.6 μm), high tolerance of ZnO ETL to defects and doping variations, and

high sensitivity of defect density of the HTL (~10^{15} cm -3), which is critically sensitive to recombination and overall efficiency.

2. Solar cell configuration and simulation methodology

2.2 Numerical Simulation using SCAPS-1D

Numerical simulations were performed using the Solar Cell Capacitance Simulator (SCAPS-1D) [13], which is a well-developed one-dimensional device simulator developed at the University of Gent. SCAPS-1D allows for the simultaneous solution of the coupled Poisson equation and the electron/hole continuity equations under steady-state conditions, thus providing a rigorous description of charge carrier transport, photogeneration, and recombination processes in multilayer photovoltaic structures. This feature allows the accurate tuning of the material and device parameters like the thickness of the layers, band gap, electron affinity, carrier mobilities, doping concentration, defect densities (both bulk and interface), recombination rates, and contact work functions without spending money on experimental processing. The motion of charge carriers in a photovoltaic device is essentially controlled by the interaction of electrostatics, generation, transport and recombination phenomena, which are quantitatively expressed in terms of a set of semiconductor equations [14].

The essence of electrostatic analysis lies in Poisson's equation, in which the spatial distribution of the electric field E in the device is linked to the local charge density ρ:

$$\frac{dE}{dx} = -\frac{\rho}{\varepsilon_s} = -\frac{q}{\varepsilon_s}\left[p - n + N_D^+(x) - N_A^-(x) \pm N_{\text{def}}(x)\right] \quad (1)$$

Here, q denotes the elementary charge, ε_s is the dielectric permittivity of the semiconductor, n and p represent the free electron and hole concentrations respectively, and N_D^+, N_A^-, and N_{def} refer to the densities of ionized donor, acceptor, and charged defect states. This equation determines the internal electric field profile, which influences carrier drift and assists in the establishment of potential barriers or wells critical for charge separation. The transport of carriers is then described by the electron and hole continuity equations. These express charge conservation by balancing spatial variations in carrier current densities (j_n for electrons, j_p for holes) with generation and recombination processes:

$$\frac{\partial j_n}{\partial x} + G - U_n(n,p) = 0 \quad (2)$$

$$-\frac{\partial j_p}{\partial x} + G - U_p(n,p) = 0 \quad (3)$$

The generation of electron-hole pair under AM1.5G irradiation is represented by G recombination rates of electrons and holes are denoted by U_n and U_p respectively. These continuity equations facilitate charge conservation by ensuring that any spatial nonuniformities in current are compensated by local generation or loss of carriers, maintaining the systematic stability of the device over time.

One of the primary recombination mechanisms in semiconductors, especially in materials with defect or trap states, is modelled by the Shockley–Read–Hall (SRH) recombination formalism. The corresponding recombination rate R_{SRH} is quantified as:

$$R_{\text{SRH}} = \frac{np - n_i^2}{\tau_p(n + n_1) + \tau_n(p + p_1)} \quad (4)$$

where n_i denotes the intrinsic carrier concentration, n_1 and p_1 are characteristic carrier concentrations related to the defect energy levels, while parameters τ_n, τ_p represent the effective carrier lifetimes for electrons and holes respectively. This relation characterises the role of defect states as recombination centres for electron-hole annihilation,

reducing the carrier population available for electrical conduction.

The carrier lifetimes (τ) themselves are determined by microscopic defect parameters:

$$\tau = \frac{1}{\sigma N_t v_{th}} \quad ,(5)$$

where σ is the defect capture cross-section, N_t describes the trap density, and v_{th} is the thermal velocity of the carriers. This expression forms a relationship between microscopic physical characteristics of defects (including their density and carrier capturing ability) and macroscopic device performance metrics like carrier lifetime and recombination rates.

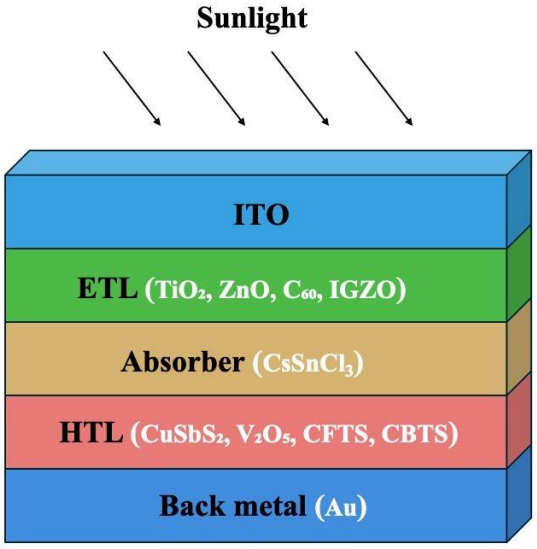

Figure 1: Schematic representation of the layer structure of the proposed $CsSnCl_3$-based perovskite solar cell architecture

2.2 $CsSnCl_3$-based Perovskite Solar Cell Structure and Energy Band Diagram

Numerical simulations of $CsSnCl_3$ perovskite solar cells (PSCs) were performed under a planar n-i-p cell geometry, in which the CsSnCl3 absorber acts as the intrinsic layer, while the hole transport layer (HTL) and electron transport layer (ETL) correspond to the p and n layers, respectively. Upon exposure to light, the CsSnCl3 perovskite material forms excitons, which disassociate effectively at the heterojunctions formed between the $CsSnCl_3$ and the HTL and ETL [13]. The electrons travel via the ETL to the ITO layer, while the holes are carried by the HTL to the Au back contact due to the presence of an electric field at the heterojunctions. The device structure used for the simulation is illustrated in Figure 1, consisting of the layered configuration ITO/ETL/$CsSnCl_3$/HTL/Au. From Figure 2 which presents the energy band alignment, it can be seen that both the electron and hole quasi-Fermi levels F_n and F_p are positioned closely to the conduction-band edge E_C and the valence-band edge, E_V within the absorber layer. While all the investigated ETLs show favourable valence-band alignment for efficient hole extraction, variations in their conduction-band edge positions lead to differences in electron extraction efficiency.

Specifically, the TiO_2, ZnO, and IGZO ETLs have comparable bandgaps, resulting in similar electron transport properties under identical simulation conditions as summarised in Table 3.

Table 1: Interface defect parameters used in the SCAPS-1D simulations

Interface	Defect Density N_{int} (cm^{-2})	Energy Level (eV)	Capture Cross-section σ (cm^2)
ETL/$CsSnCl_3$	1×10^{12}	Mid-gap	1×10^{-15}
$CsSnCl_3$/HTL	1×10^{12}	Mid-gap	1×10^{-15}

The front contact, ITO, possesses a work function of 4.0 eV, optimizing electron collection, whereas the Au back contact, with a work function of 5.1 eV, efficiently collects holes from the HTL. A comprehensive screening of multiple ETL and HTL materials was performed, testing 16 combinations with $CsSnCl_3$ fixed as the absorber. The combinations were evaluated based on photovoltaic metrics such as power conversion efficiency, open-circuit voltage, short-circuit current density, and fill factor.

The most promising ETL/HTL pairs were further optimized for thickness, doping, and defect densities. Interface defect densities at each heterojunction were also incorporated as

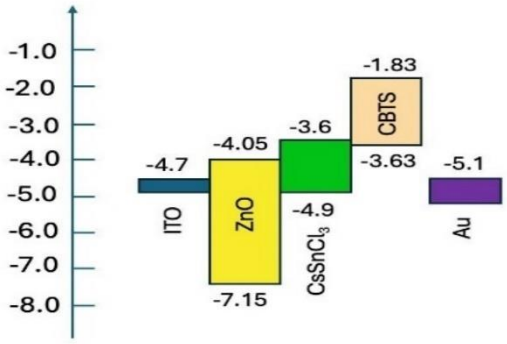

Figure 2: Simulated energy band alignment for the optimized solar cell as investigated

summarized in Table 1. All simulations were conducted at a temperature of 300 K under AM1.5G solar illumination with an incident power density of 100 mW/cm^2, providing a realistic operational environment for the device performance assessment.

In addition to bulk defect densities, the effects of interface defect states at the ETL/perovskite and perovskite/HTL junctions were incorporated to accurately model recombination losses. Table 1 summarizes the interface defect densities, their energy levels, and capture cross-sections used in the simulations.

2.3 Simulation Strategy

The computational workflow comprised four sequential optimisation stages:

Stage 1: ETL/HTL combinatorial screening. All 16 ETL/HTL combinations were simulated for a fixed absorber configuration. Key photovoltaic parameters - namely power conversion efficiency (PCE), open-circuit voltage (V_{OC}), short-circuit current density (J_{SC}), and fill factor (FF) - were analysed, and the highest-performing ETL/HTL combination was selected.

Stage 2: Thickness optimization. Following the identification of the optimal ETL/HTL pair, the thicknesses of the ETL, absorber, and HTL were varied independently (ETL: 10–50 nm; absorber: 100–600 nm; HTL: 20–60 nm). The configuration yielding the highest PCE was retained.

Stage 3: ETL doping and defect tuning. The optimized thickness configuration was subsequently further evaluated by varying the ETL donor doping concentration (N_D, 10^{15}–10^{20} cm^{-3}) and ETL bulk defect density (N_t, 10^{10}–10^{15} cm^{-3}). The effects on V_{OC}, J_{SC}, FF, and PCE were monitored to identify optimal electronic properties.

Stage 4: HTL optimization. An identical doping/defect tuning process was applied to the HTL acceptor doping (N_A) and defect density.

Stage 5: Perovskite Optimization The donor density doping concentration and defect density of the perovskite $CsSnCl_3$ layer.

Table 2: Input parameters for the $CsSnCl_3$ absorber layer used in SCAPS-1D simulations

Parameter	Value
Thickness (nm)	500
Bandgap E_g (eV)	1.45
Electron affinity χ (eV)	4.10
Relative permittivity ε_r	15
Effective density of states in conduction band N_C (cm^{-3})	2.0×10^{18}
Effective density of states in valence band N_V (cm^{-3})	1.8×10^{19}
Electron mobility μ_n (cm^2/Vs)	20
Hole mobility μ_p (cm^2/Vs)	20
Intrinsic doping concentration N_i (cm^{-3})	1.0×10^{10}
Bulk defect density N_t (cm^{-3})	1.0×10^{14}
Capture cross-section σ (cm^2)	1.0×10^{-15}

2.4 Input Parameters

The key physical and electronic parameters of the $CsSnCl_3$ absorber used in the simulations are summarized in Table 2. These include the bandgap, electron affinity, dielectric constant, carrier mobilities, intrinsic doping levels, and defect densities, which critically influence the device performance Baseline parameters including bandgap, electron affinity, dielectric constant, carrier mobilities, doping concentrations, and defect densities were taken from experimental reports and validated simulations (Table 3).

3. Results and Discussion

3.1 Combinatorial Screening of Heterojunction Architectures

To identify an optimal device structure for $CsSnCl_3$ perovskite solar cells, we tried a combinatorial screening approach of 16 potential heterojunctions outlined in table. In this, different combinations of electron transport layers (ETLs) and hole transport layers (HTLs) were screened in a systematic way, keeping the $CsSnCl_3$ as absorber layer.

Four ETLs, IGZO, ZnO, TiO_2, and C_{60}, and four HTLs, CBTS, CFTS, V_2O_5, and $CuSbS_2$, were studied, which gave rise to 16 unique heterojunction configurations. All of the structures were simulated through the same boundary condition, interface parameter, and carrier transport property, enabling direct comparability of the V_{OC}, J_{SC}, FF, and η. The combinatorial screening serves to identify ETL/HTL pairs that maximise charge carrier extraction and minimise recombination losses as well as understand material dependent effects on device performance, including energy level alignment, carrier mobility, and interfacial recombination.

The results of the screening are summarised in Table 4. Of the configurations that were examined, the ZnO/$CsSnCl_3$/CBTS module yields the maximum balanced performance with V_{OC} = 0.7893 V, J_{SC} = 16.56 $mAcm^{-2}$, FF = 61.68%, and η = 7.15%. Devices constituting of V_2O_5 or $CuSbS_2$ as the HTL display prominent reductions in J_{SC} and efficiency which can be explained by increased interfacial recombination and inadequate energy alignment. Devices consisting of C_{60}-based ETLs exhibit moderate performance, primarily limited by the lower electron mobility of ZnO. Conversely, the TiO_2/$CsSnCl_3$/CBTS architecture achieves a similar efficiency of 7.14%, with a lower V_{OC} (0.5646 V) compensated by a higher J_{SC} (21.05 mA/cm^2). This demonstrates increased photon absorption but less favourable band alignment for effective voltage generation.

Table 3: Baseline input parameters for the Hole Transport Layer (HTL) and Electron Transport Layer (ETL) used in SCAPS-1D simulations.

Parameter		HTL				ETL		
	$CuSbS_2$	V_2O_5	CFTS	CBTS	TiO_2	ZnO	C_{60}	IGZO
Thickness (nm)	100	100	100	100	100	100	100	100
E_g (eV)	1.58	2.20	1.30	1.90	3.20	3.30	1.70	3.05
Electron affinity χ (eV)	4.20	4.00	3.30	3.60	4.00	4.00	3.90	4.16
ε_r	14.6	10	9	5.4	9	9	4.2	10
NC (cm^{-3})	2.0×10^{18}	9.2×10^{17}	2.2×10^{18}	2.2×10^{18}	2.0×10^{18}	3.7×10^{18}	8.0×10^{19}	5.0×10^{18}
NV (cm^{-3})	1.0×10^{19}	5.0×10^{18}	1.8×10^{19}	1.8×10^{19}	1.8×10^{19}	1.8×10^{19}	8.0×10^{19}	5.0×10^{18}
$v_{th,e}$ (cm/s)	1.0×10^{7}	1.0×10^{7}	1.0×10^{7}	1.0×10^{7}	1.0×10^{7}	1.0×10^{7}	1.0×10^{7}	1.0×10^{7}
$v_{th,h}$ (cm/s)	1.0×10^{7}	1.0×10^{7}	1.0×10^{7}	1.0×10^{7}	1.0×10^{7}	1.0×10^{7}	1.0×10^{7}	1.0×10^{7}
μ_n (cm^2/Vs)	49	3.2×10^{2}	21.98	30	20	100	8.0×10^{-2}	15
μ_h (cm^2/Vs)	49	4.0×10^{1}	21.98	10	10	25	3.5×10^{-3}	0.1
ND (cm^{-3})	0	0	0	0	9.0×10^{16}	1.0×10^{18}	1.0×10^{17}	1.0×10^{17}
NA (cm^{-3})	1.0×10^{18}	1.0×10^{18}	1.0×10^{18}	1.0×10^{18}	0	0	0	0
Nt (cm^{-3})	1.0×10^{15}	1.0×10^{15}	1.0×10^{15}	1.0×10^{15}	1.0×10^{15}	1.0×10^{15}	1.0×10^{15}	1.0×10^{15}

Table 4: Photovoltaic performance of different ETL/HTL combinations with $CsSnCl_3$ as the absorber.

Structure	V_{OC} (V)	J_{SC} (mA/cm^2)	FF (%)	η (%)
ZnO/$CsSnCl_3$/CBTS	0.7893	16.557014	61.68	7.15
ZnO/$CsSnCl_3$/CFTS	0.7902	16.565508	59.78	7.12
ZnO/$CsSnCl_3$/V_2O_5	0.5685	7.69E-01	63.34	0.28
ZnO/$CsSnCl_3$/$CuSbS_2$	0.4539	13.714259	45.75	2.85
TiO_2/$CsSnCl_3$/CBTS	0.5646	21.05632	60.03	7.14
TiO_2/$CsSnCl_3$/CFTS	0.5974	17.413918	56.00	5.83
TiO_2/$CsSnCl_3$/V_2O_5	0.3573	1.294983	63.32	0.29
TiO_2/$CsSnCl_3$/$CuSbS_2$	0.4492	14.276164	54.15	3.47
C_{60}/$CsSnCl_3$/CBTS	0.4224	25.076002	60.49	6.41
C_{60}/$CsSnCl_3$/CFTS	0.5730	19.916864	61.14	6.98
C_{60}/$CsSnCl_3$/V_2O_5	0.3405	6.61E-01	63.65	0.14
C_{60}/$CsSnCl_3$/$CuSbS_2$	0.2035	12.820296	53.92	1.41
IGZO/$CsSnCl_3$/CBTS	0.6642	19.304565	50.63	6.49
IGZO/$CsSnCl_3$/CFTS	0.7348	15.597707	59.31	6.80
IGZO/$CsSnCl_3$/V_2O_5	0.3698	2.260451	61.41	0.51
IGZO/$CsSnCl_3$/$CuSbS_2$	0.2006	11.306041	52.33	1.19

Promising J_{SC} values are obtained for C_{60} based modules, notably C_{60}/$CsSnCl_3$/CBTS (25.08 mA/cm^2), However, they are hindered by low V_{OC} (0.4224 V), which result in lower PCE outputs. IGZO-based configurations tend to be underperforming due to reduced FF and divergent energy levels, while V_2O_5 and $CuSbS_2$ HTLs exhibit extremely low efficiencies, arising

from poor band alignment and high recombination rates.

These results indicate ZnO as the optimal ETL and CBTS as the optimal HTL, setting a baseline for further layer-specific optimization. The combinatorial approach efficiently informs experimental design, that resources be directed to optimize promising material combinations to obtain high-performance $CsSnCl_3$ heterojunction solar cells.

3.2 Thickness Optimisation Thickness optimisation of the Absorber Layer – $CsSnCl_3$

Here, perovskite absorber layer thickness optimisation within $CsSnCl_3$/ZnO heterojunction solar cell has been carried out in order to study absorber layer thickness-dependent performance parameter behavior. The property parameters of all the layers are held constant as specified in Tables 1 and 2, and flat-band ohmic contacts are assumed both at front and back sides. The $CsSnCl_3$ layer is tested with a doping concentration of × 1015 cm^{-3} while the ZnO ETL thickness is maintained at its optimal value. The thickness of the perovskite absorber layer is varied from 0.1 to 0.6 µm. Figure 4 depicts the photovoltaic parameter variation with absorber thickness. For thicknesses ranging from 0.1 to 0.3 µm, both V_{OC} and J_{SC} show a considerable rise. Values for V_{OC} increases from 0.6401 V to 0.7326 V, and J_{SC} increases from 16.34 to 22.47 mA cm^{-2}. This trend owes to the directly proportional relation between absorber thickness and photon absorption and carrier generation. However, beyond ~0.6 µm, recombination and transport losses begin to offset the gains from greater thickness, thereby diminishing efficiency improvements. Thicknesses exceeding 0.3 μm, provide declining but still useful returns. At 0.6 μm, V_{oc} is 0.7658 V, J_{sc} is 25.29 mA cm^{-2}, and FF increases from 68.37% at 0.1 μm to 78.87%, indicative of lower recombination and improved transport of carriers. These collective gains lead to a maximum efficiency of 15.27% at 0.6 μm, over twice the amount realized at 0.1 μm (7.15%). We observed that an increase in perovskite thickness from 0.6 μm would only give rise to marginal increases in performance due to likely recombination within the absorber and resistance losses within the ETL.

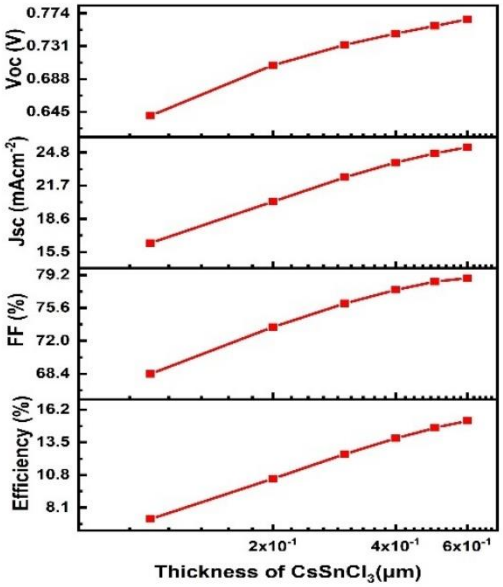

Figure 3: Variation of V_{oc}, J_{sc}, fill factor, and efficiency with thickness of the $CsSnCl_3$ layer

Consequently, forward in order to obtain optimal performance as tabulated in Table 5. An optimised 0.6 μm perovskite thickness is put for the $CsSnCl_3$/ZnO heterojunction solar cell,

3.3 Thickness optimisation of the Electron Transport Layer ZnO

Systematically, thickness optimisation of the ZnO electron transport layer (ETL) of the $CsSnCl_3$/ZnO/CBTS heterojunction solar cell has been studied. All other layer parameters, such as the perovskite absorber and the CBTS hole transport layer, remained as before, and flat-band ohmic contacts were used at each electrode. Thickness optimisation is paramount because each layer's performance hinges on balancing photo-generated carrier diffusion length, lifetime, and mobility, which determine

charge separation across the heterojunction, recombination in the material concentration was maintained at 1 × 10^{15} cm^{-3}. The ZnO thickness was changed between 0.01 μm and 0.05 μm.

Figure 3 and Table 4 illustrate the device performance trends with varying thickness of the ZnO layer. From 0.01 μm to 0.03 μm, V_{oc} slightly rises from 0.7674 V to 0.7683 V due to enhanced electron blocking at the perovskite/HTL interface, minimizing the chances of hole back-transfer and maximizing built-in potential. J_{sc} shows only a very small drop from 25.496 mA cm^{-2} to 25.491 mA cm^{-2}, which suggests that the ZnO layer is still highly transparent over this range, with little optical loss and only slightly longer electron transport distances.

The fill factor (FF) decreases slightly from 79.87% to 79.66% over the same range, presumably a result of minute increases in series resistance created by thicker ETL. In spite of this, the PCE is maximized at 15.61% at 0.03 μm, the best compromise between enhanced voltage and containable resistive losses. While further increases in ZnO thickness, above 0.03 μm, lead to incremental losses in V_{oc} (to 0.7694 V at 0.05 μm) as well as larger FF losses (to 78.96%), smaller losses in J_{sc} (to 25.482 mA cm^{-2}) accompany these losses. This performance deterioration is due to higher series resistance as well as possible carrier recombination inside the ETL, which start restricting charge extraction efficiency.

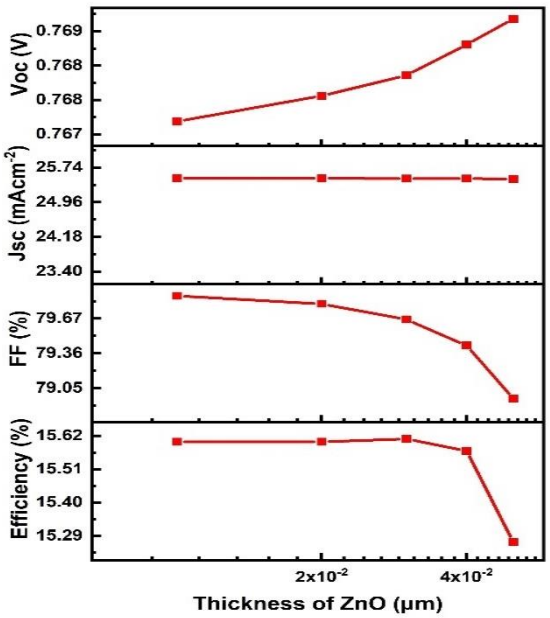

Figure 4: Variation of V_{oc}, J_{sc}, fill factor, and efficiency with thickness in the ZnO Layer.

The PCE drops to 15.27% at 0.05 μm, supporting the fact that thicker ETLs can degrade instead of improve overall performance.

On the basis of these findings, an optimised thickness of 0.03 μm for ZnO ETL is suggested since it provides the optimal compromise between the improved separation of charges, reduced resistive loss, and negligible optical attenuation and thus maximises efficiency in the $CsSnCl_3$/ZnO heterojunction solar cell.

Table 5: Thickness of perovskite absorber layer and photovoltaic performance.

Thickness (μm)	**V_{oc} (V)**	**J_{sc} (mA/cm^2)**	**FF (%)**	**η (%)**
0.1	0.6401	16.343394	68.37	7.15
0.2	0.7061	20.207083	73.5	10.49
0.3	0.7326	22.465648	76.07	12.52
0.4	0.7473	23.841284	77.56	13.82
0.5	0.7574	24.713258	78.46	14.69
0.6	0.7658	25.285758	78.87	15.27

3.4. *Thickness optimisation of the Hole Transport Layer (HTL) – CBTS*

The optimisation of the CBTS (Cu_2BaSnS_4) hole transport layer of the $CsSnCl_3$/CBTS heterojunction solar cell was conducted to evaluate the effect of varying the thickness of the HTL on the important performance parameters. The simulation parameters for all the layers were kept as stipulated in Tables 1 and 2, with flat-band ohmic contacts at both the front and rear interfaces. Perovskite absorber and ZnO ETL were both set at their respective optimised thickness levels, and the CBTS doping concentration was also maintained the same as the optimised setup. The CBTS thickness ranged from 0.02 μm to 0.06 μm.

Figure 5 and Table 6 present the ensuing photovoltaic trends. With increasing CBTS thickness from 0.02 μm to 0.04 μm, V_{oc} improved consistently from 0.7565 V to 0.7613 V. This is because improved interface coverage at the CBTS/perovskite junction decreases interfacial trap density and suppresses non-radiative recombination. J_{sc} improved from 25.005 mA cm^{-2} to 25.292 mA cm^{-2} at the same time which indicates more efficient hole extraction and less carrier backflow towards the absorber. Nonetheless, within the aforementioned range, the fill factor (FF) exhibited a slight reduction from 83.09% at a thickness of 0.02 μm to 81.3% at a thickness of 0.04 μm. This limited decrease can be attributed to increased series resistance with thicker HTL layers that compromises charge transport to some extent, despite improvement in interfacial quality.

Hence, a modest but noticeable improvement was observed for the PCE, reaching 15.65% at the thickness of 0.04 μm that is, a balanced compromise among charge separation, transport efficiency, and resistive losses. However, when increasing from thicknesses more than 0.04 µm to 0.06 µm, there were some reductions in effectiveness. The open circuit voltage value was sustained but at an increased level of 0.7682 V while short circuit current density value was maintained at 25.492 mA cm^{-2} indicating further improvements in optical absorption and hole collection. FF fell more significantly to 79.72%, presumably a consequence of increasing cumulative resistive losses and enhanced probability of recombination in the thicker HTL. Consequently, PCE dropped marginally to 15.61% at 0.06 μm.

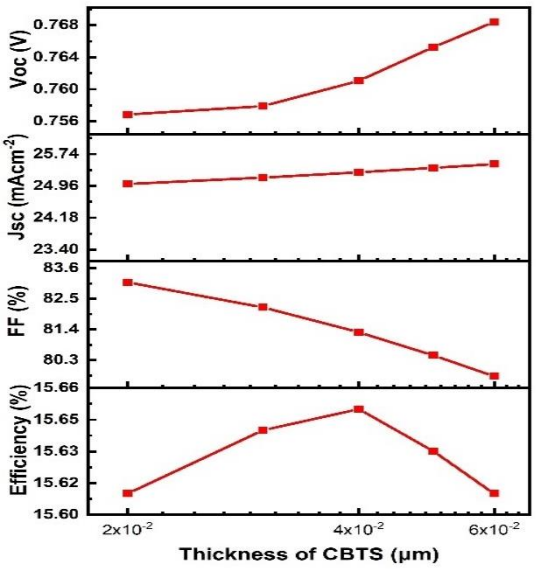

Figure 5: Variation of V_{oc}, J_{sc}, fill factor, and efficiency with thickness in the CBTS Layer.

Table 5: Thickness of perovskite absorber layer and photovoltaic performance.

Thickness (μm)	**V_{oc} (V)**	**J_{sc} (mA/cm^2)**	**FF (%)**	**η (%)**
0.01	0.7674	25.496096	79.87	15.60
0.02	0.7679	25.493633	79.80	15.60
0.03	0.7683	25.490602	79.66	15.61
0.04	0.7689	25.486913	79.43	15.57
0.05	0.7694	25.481651	78.96	15.27

As a whole, the results show that although incremental V_{oc} and J_{sc} improvements can be gained through increasing the thickness of the CBTS layer, the accompanying FF decrease counteracts these advantages. The optimal thickness of the CBTS layer is found to be 0.04 μm, where the device has its maximum simulated efficiency of 15.65% with a desirable balance between electrical and optical performance.

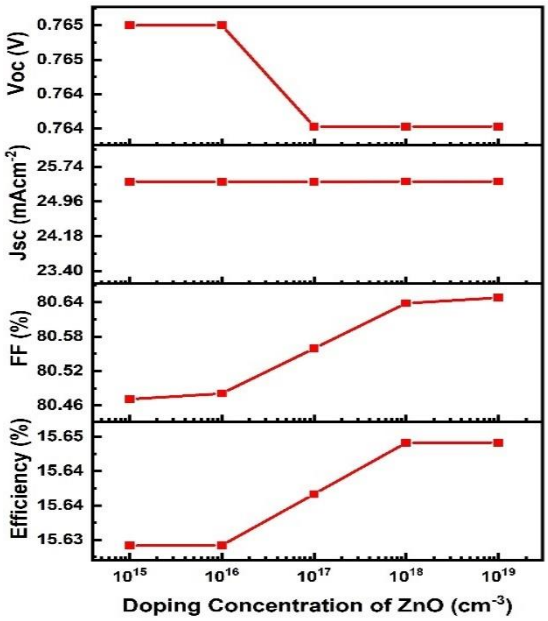

Figure 6: Variation of V_{oc}, J_{sc}, fill factor, and efficiency with doping concentration in the ZnO Layer.

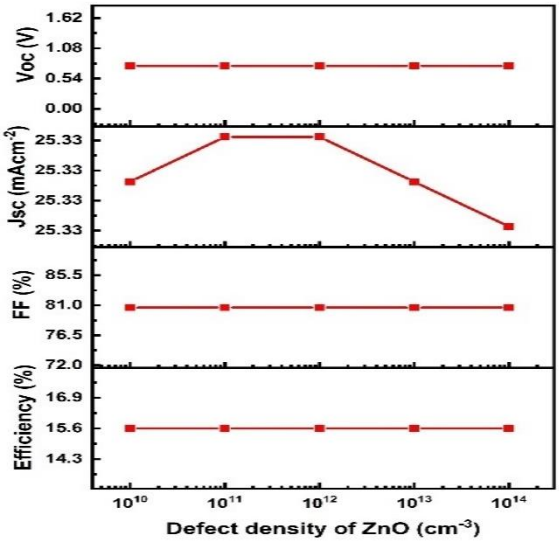

Figure 7: Variation of photovoltaic parameters — (a) open-circuit voltage (V_{oc}), (b) short-circuit current density (J_{sc}), (c) fill factor (FF), and (d) power conversion efficiency (PCE) as a function of ZnO electron transport layer doping concentration in the $CsSnCl_3$-based perovskite solar cell

.

Table 7: Thickness of CBTS HTL and photovoltaic performance.

Thickness (μm)	V_{oc} (V)	J_{sc} (mA/cm^2)	FF (%)	η (%)
0.02	0.7565	25.005136	83.09	15.61
0.03	0.7581	25.160604	82.19	15.64
0.04	0.7613	25.291760	81.30	15.65
0.05	0.7648	25.401410	80.47	15.63
0.06	0.7682	25.491622	79.72	15.61

3.4.1 ZnO Layer Doping and Defect Density Optimisation

The influence of defect density and donor density on the performance of the ZnO electron transport layer (ETL) in $CsSnCl_3$/ZnO/CBTS heterojunction solar cells was comprehensively examined. All the previously optimised parameters for the perovskite absorber (0.6 μm) and CBTS hole transport layer (0.04 μm) were kept constant, while having flat band ohmic contacts at both electrodes. Donor concentration of ZnO was changed from 1×10^{15} cm^{-3} to 1×10^{20} cm^{-3} and defect concentration was changed from 1×10^{10} cm^{-3} to 1×10^{15} cm^{-3} in order to investigate their impact on open-

circuit voltage (V_{oc}), short-circuit current density (J_{sc}), fill factor (FF), and power conversion efficiency (η).

Figure 6 shows the donor density dependence of the performance parameters. The invariance of Voc with ZnO donor density indicates that the built-in electric field is primarily governed by band alignment rather than ETL doping, confirming that ZnO functions mainly as a charge transport layer rather than a junction-forming layer. J_{sc} varies very little (≈ 25.40–25.41 mA cm^{-2}), which means carrier generation and transport are not much affected by the donor concentration over this range. The fill factor (FF) is seen to improve marginally with an increase in donor density, implying that there is marginal improvement in charge transport but decreased resistive loss. This translates into the efficiency η improving minimally from 15.63% at 1×10^{15} cm^{-3} to 15.65% at 1×10^{20} cm^{-3}. There is also no influence from variations in defect density of ZnO in the cell performance. For example, the efficiency of ≈ 15.6%. This suggests that ZnO ETL is insensitive to intrinsic defect levels within the measured range, indicating strong the ranges considered for donor and defect densities, ZnO displays stable electronic properties, providing reliable V_{oc}, J_{sc}, and FF.

The results indicate that while J_{sc} remains nearly constant, FF and PCE increase with higher doping concentration, whereas V_{oc} slightly decreases beyond 10^{16} cm^{-3} slight variations in doping or defects will not significantly reduce device performance, making it easier to fabricate while retaining high efficiency carrier transport and low trap-assisted recombination in such conditions. In short, in V_{OC}, J_{SC}, and (FF) remain unchanged at around 0.7636 V, 25.33 mA cm^{-2}, and 80.65%, respectively, leading to an effectively constant The results show that J_{sc} remains nearly constant, while V_{oc}, FF, and PCE exhibit a sharp increase at doping concentrations above 10^{14} cm^{-3}.

3.4.2 CBTS Layer Doping and Defect Density Optimization

The effect of acceptor density and defect density on the performance of the CBTS hole transport layer (HTL) was systematically investigated while keeping all the previously optimized parameters such as $CsSnCl_3$

Table 8: Optimized performance parameters corresponding to ZnO donor and defect density

ZnO Parameter	V_{oc} **[V]**	J_{sc} **[mAcm^{-2}]**	**FF [%]**	η **[%]**
Donor Density 1×10^{15}	0.7648	25.40141	80.47	15.63
Donor Density 1×10^{16}	0.7647	25.40166	80.48	15.63
Donor Density 1×10^{17}	0.7644	25.40322	80.56	15.64
Donor Density 1×10^{18}	0.7640	25.40567	80.64	15.65
Donor Density 1×10^{19}	0.7638	25.40638	80.65	15.65
Donor Density 1×10^{20}	0.7637	25.40577	80.65	15.65
Defect Density 1×10^{10}	0.7636	25.33054	80.65	15.60
Defect Density 1×10^{11}	0.7636	25.33054	80.65	15.60
Defect Density 1×10^{12}	0.7636	25.33054	80.65	15.60
Defect Density 1×10^{13}	0.7636	25.33054	80.65	15.60
Defect Density 1×10^{14}	0.7636	25.33054	80.65	15.60
Defect Density 1×10^{15}	0.7636	25.33053	80.65	15.60

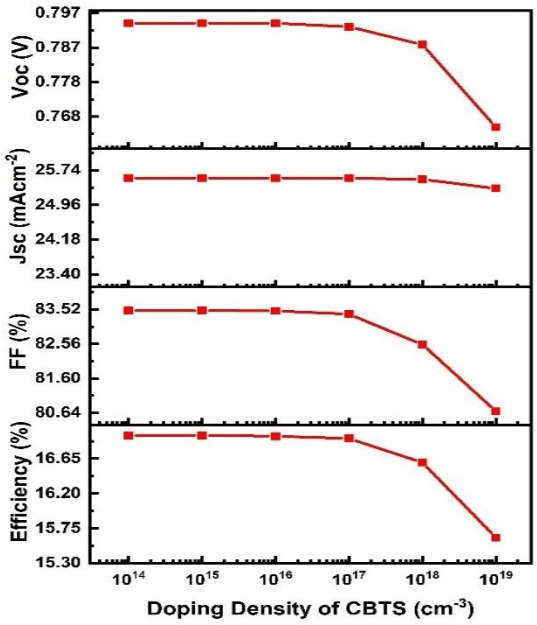

Figure 8: Variation of photovoltaic parameters — (a) open-circuit voltage (V_{oc}), (b) short circuit current density (J_{sc}), (c) fill factor (FF), and (d) power conversion efficiency (PCE) as a function of CBTS hole transport layer doping concentration in the $CsSnCl_3$-based perovskite solar cell.

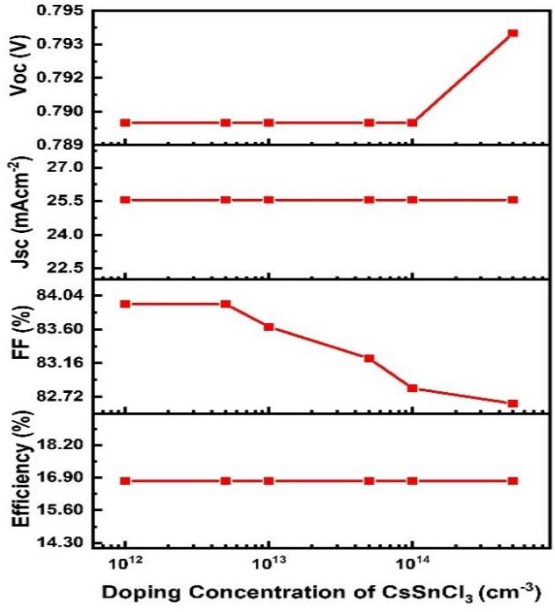

Figure 9: Influence of CBTS hole transport layer doping density on photovoltaic parameters — (a) open-circuit voltage (V_{oc}), (b) short-circuit current density (J_{sc}), (c) fill factor (FF), and (d) power conversion efficiency (PCE) — in $CsSnCl_3$-based perovskite solar cells.

perovskite thickness of 0.6 µm and ZnO ETL thickness of 0.03 µm. Flat-band ohmic contacts were assumed at both the electrodes. The density of acceptor in CBTS was tuned between 5 × 109 cm^{-3} to 5 × 1014 cm^{-3}, and defect density was tuned between 1 × 1014 cm^{-3} to 1 × 1019 cm^{-3} to analyse their effect on open-circuit voltage (Voc), short-circuit current density (Jsc), fill factor (FF), and power conversion efficiency (η). By comparison, the defect density of CBTS significantly impacts device performance. With the increase of defect density from 1 × 1014 cm^{-3} to 1 × 1015 cm^{-3}, Voc and FF rise

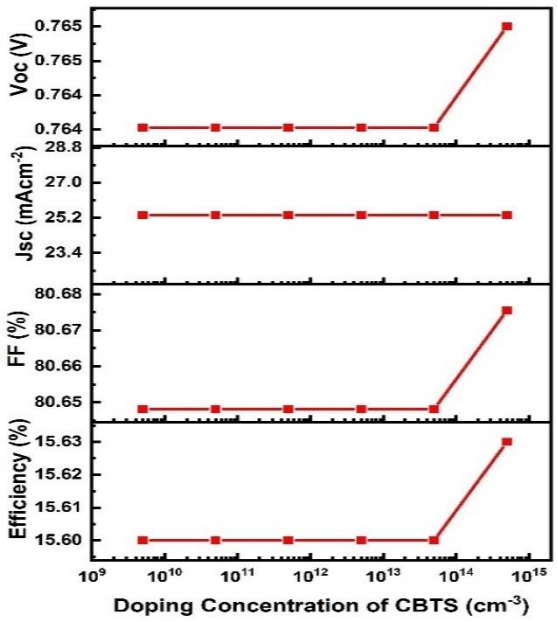

Figure 10: Effect of $CsSnCl_3$ absorber layer doping concentration on photovoltaic characteristics: (a) open-circuit voltage (V_{oc}), (b) short-circuit current density (J_{sc}), (c) fill factor (FF), and (d) power conversion efficiency (PCE).

to peaks of 0.7941 V and 83.49%, respectively. This is accompanied by an efficiency peak of 16.95%. The initial rise may be because of better band alignment and less interfacial trap-assisted recombination, leading to better charge extraction. However, after 1 × 1015 cm^{-3}, the performance decreases step by step: Voc reduces to 0.7651 V at 1 × 1019 cm^{-3}, FF reduces to 80.68%, and η returns to 15.63%. The observed performance degradation at higher defect densities confirms that trap-

assisted Shockley–Read–Hall recombination dominates in the HTL, reducing carrier lifetime and suppressing both fill factor and open-circuit voltage. Surprisingly, Jsc is quite stable (~ 25.33–25.56 $mAcm^{-2}$) across the entire defect density range, suggesting that the density of photogenerated carriers is not appreciably influenced.

The findings show that although the density of CBTS acceptors affects the performance of the device to a small extent, defect density becomes the major parameter for controlling Voc, FF, and efficiency. An optimal defect density of 1×10^{15} cm^{-3} maximises efficient hole transport and reduces recombination contributing to the greater efficiency. Therefore, this emphasises the significance of the interface and bulk defect engineering of HTLs in the fabrication of perovskite solar cells. Thus, keeping defect density within the optimal value range is crucial for achieving high-performing $CsSnCl_3$/ZnO/CBTS heterojunction solar cells. An increase in doping concentration above 1×10^{13} cm^{-3} leads to a significant rise in V_{oc}, while J_{sc} and PCE are practically unaffected by the change in doping level. The fill factor shows a monotonic decrease with increasing doping concentration levels.

3.5 Perovskite Layer Doping and Defect Density Optimization

The present subsection considers the impact of acceptor density and defect density on the performance of the $CsSnCl_3$ perovskite in the $CsSnCl_3$/ZnO/CBTS solar cell. All the previously optimised parameters for the ZnO ETL and CBTS HTL are kept constant. The thickness of the perovskite absorber layer is constant at 0.6μm, with flat-band ohmic contacts existing at every electrode junction. Acceptor concentration is varied between 1×10^{12} cm^{-3} to 5×10^{14} cm^{-3}, and defect concentration is varied between 1×10^{10} cm^{-3} to 1×10^{15} cm^{-3}. The impact of variations in acceptor density on open circuit voltage (V_{oc}), short-circuit current density (J_{sc}), fill factor (FF), and total power conversion efficiency (η) is investigated. According to Figure **10**, as acceptor concentration rises from 1×10^{12} cm^{-3} to 5×10^{14} cm^{-3}, open circuit voltage also increases from 0.7897V to 0.7942V respectively. This phenomenon can be associated with improved internal electric field strength due to higher doping concentrations, leading to higher efficiency in separating charges at the perovskite/ZnO interface. At the same time, no significant change is observed for J_{sc} which remains almost constant at ~ 25.56 mA cm^{-2}, suggesting that photogeneration rate and carrier extraction are insensitive to variations in acceptor density over this range. A slight reduction in FF is found, ranging between 83.93% and 82.63%, which can be attributed to increased series resistance and reduced carrier mobility that accompany higher doping levels. Consequently, η remains constant at ~ 16.77%, highlighting that moderate acceptor density tuning can successfully balance the trade-off between high open circuit voltage and high recombination losses, thus ensuring stable overall device performance. Increasing defect density above 10^{13} cm^{-3} results in a sharp increase in V_{oc}, while J_{sc} remains relatively constant. FF and PCE exhibit a notable decline at higher defect densities mainly enhances V_{oc} without negatively affecting J_{sc} or FF. This proves that $CsSnCl_3$ layers are endowed with adequate intrinsic hole conductivity for effective carrier transport even under lower concentrations of doping. The identified defect density of the $CsSnCl_3$ layer significantly influences the performance, as shown in Figure 11. At defect densities ranging from low (1×10^{10}–1×10^{13} cm^{-3}), V_{oc} is considerable (~ 0.7942V), J_{sc} does not change much (~ 25.56$mAcm^{-2}$), and FF is around 83.4–83.5%, resulting in maximum efficiency of 16.95%

Table 9: Optimum performance parameters of CBTS acceptor and defect densities

CBTS Parameter	V_{oc} **[V]**	Jsc **[mAcm^{-2}]**	**FF [%]**	η **[%]**
Acceptor Density 5 × 10^{9}	0.7636	25.33054	80.65	15.60
Acceptor Density 5 × 10^{10}	0.7636	25.33054	80.65	15.60
Acceptor Density 5 × 10^{11}	0.7636	25.33054	80.65	15.60
Acceptor Density 5 × 10^{12}	0.7636	25.33052	80.65	15.60
Acceptor Density 5 × 10^{13}	0.7637	25.33038	80.65	15.60
Acceptor Density 5 × 10^{14}	0.7651	25.32889	80.68	15.63
Defect Density 1 × 10^{14}	0.7941	25.55971	83.49	16.95
Defect Density 1 × 10^{15}	0.7941	25.55969	83.49	16.95
Defect Density 1 × 10^{16}	0.7940	25.55942	83.48	16.94
Defect Density 1 × 10^{17}	0.7934	25.55677	83.39	16.91
Defect Density 1 × 10^{18}	0.7878	25.53094	82.54	16.60
Defect Density 1 × 10^{19}	0.7651	25.32889	80.68	15.63

This indicates very little non-radiative recombination and effective carrier extraction. However, at high defect concentrations, especially 1 × 10^{15} cm^{-3}, FF dramatically decreases to 76.73%, with η also decreasing to 15.62%, even when V_{oc} is slightly increased to 0.8013V. This decrease is caused by increased trap-assisted non-radiative recombination that raises carrier loss and caps extraction efficiency at contacts. J_{sc} likewise exhibits a small drop, role. indicating smaller effective carrier collection. Hence, defect density is an important limiting factor in high-efficiency perovskite solar cells, with defect passivation strategies playing a vital role. These ranges ensure a balance between enhanced V_{oc} and high FF while minimising recombination losses, resulting in optimal efficiency of ~ 16.95%. The results show that though V_{oc} can be slightly improved through enhanced acceptor density, FF and η are mostly influenced by the density of defects. The utilisation of perovskite layers with low defect density (< 1×10^{14} cm^{-3}) is a key factor necessary for ensuring efficient carrier transport and maximum efficiency. The results show the need for high accuracy in material quality control and effective defect passivation in $CsSnCl_3$-based perovskite solar cells.

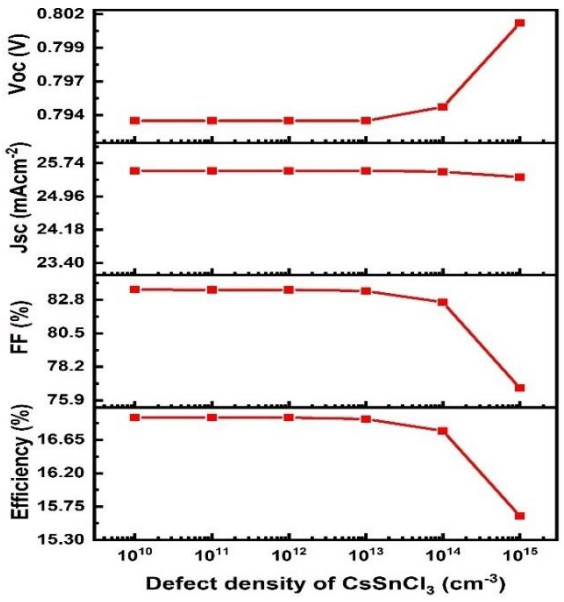

Figure 11: Influence of $CsSnCl_3$ absorber layer defect density on photovoltaic performance parameters V_{oc}, J_{sc}, FF, and PCE.

3.6 Optimised Device Parameters and Interface Properties

Despite being more efficient than most experimentally determined efficiencies of $CsSnCl_3$-based solar cells, it represents a theoretical maximum obtained under optimized and defect-minimized simulation conditions. In practical scenarios, factors such as interface imperfections, material instability, and fabrication constraints are expected to reduce achievable efficiencies.

These findings contribute to the advancement of lead free perovskite based solar cell development and computational photovoltaic modelling for a more sustainable future. Interface defect characteristics for the heterojunctions are summarized in Table 11. The optimized interface properties and layer parameters as a whole support the superior performance of the device. The ZnO ETL facilitates effective electron extraction and reduces recombination due to its low defect concentration and high electron mobility. The $CsSnCl_3$ perovskite absorber has strong absorption in the optical range, with an acceptor density that is well controlled and very few intrinsic defects, thus improving carrier lifetime and diffusion length. In the meantime, the CBTS HTL ensures effective hole transport and extraction while minimizing recombination at the perovskite/HTL interface. In addition, the interface defect densities are minimized to 1×10^{10} cm^{-3}, successfully avoiding trap-assisted recombination at the heterojunctions.

This optimisation of layer thickness, band alignment, carrier mobility, doping concentration, and defect densities leads to an optimised trade-off among V_{oc}, J_{sc}, and FF, resulting in a power conversion efficiency of 16.95%. The results highlight the need for accurate material and interface engineering for the realization of high-performance perovskite-based heterojunction solar cells. In summary, our work optimised lead-free $CsSnCl_3$ solar cells with a *n-i-p* heterostructure systematically using SCAPS-1D for a wide range of possible electron transport layers (ETLs) and hole transport layers (HTLs). A range of heterostructures within the ITO/ETL/$CsSnCl_3$/HTL/Au architecture were assessed and the most efficient module from 16 possible combinations with TiO_2, ZnO, C_{60}, and IGZO as ETLs and $CuSbS_2$, V_2O_5, CFTS, and CBTS as HTLs was optimised to identify structures yielding the highest performance. This research exhibits the potential of Pb-free $CsSnCl_3$ perovskite as an absorber layer for highly efficient PSCs. The optimisation of the PSC heterostructure by SCAPS-1D numerical simulation software showed that the combination of ZnO as electron transport layer, and CBTS as hole transport layer gave the highest PCE of 16.95%. To contextualize the obtained results, previously reported studies on tin-based and chloride perovskite solar cells typically demonstrate efficiencies in the range of ~5–12% in simulation and generally lower in experimental implementations [7,9,13]. The higher efficiency achieved in this work is attributed to systematic multi-parameter optimization, including minimized interface defect densities (~10^{10} cm^{-3}) and idealized band alignment. Therefore, the present results should be interpreted as a theoretical performance ceiling rather than a directly achievable experimental benchmark.

Table 10: Key material parameters of each functional layer.

Layer Parameter	ZnO	$CsSnCl_3$	CBTS
Thickness (μm)	0.027	0.646	0.05
Bandgap (eV)	2.527	1.558	1.4
Electron Affinity (eV)	3.5	3.8	3.65
Dielectric Permittivity	3	15.4	5.4
CB Effective DOS (cm^{-3})	3.7×10^{18}	1×10^{19}	2.2×10^{18}
VB Effective DOS (cm^{-3})	1.8×10^{19}	1×10^{19}	1.8×10^{19}
Electron Thermal Velocity ($cm\ s^{-1}$)	1×10^{7}	1×10^{7}	1×10^{7}
Hole Thermal Velocity ($cm\ s^{-1}$)	1×10^{7}	1×10^{7}	1×10^{7}
Electron Mobility ($cm^2\ V^{-1}\ s^{-1}$)	100	2	30
Hole Mobility ($cm^2\ V^{-1}\ s^{-1}$)	25	2	10
Shallow Donor Density N_D (cm^{-3})	1×10^{22}	0	0
Shallow Acceptor Density N_A (cm^{-3})	0	9×10^{14}	5.5×10^{14}
Defect Density (cm^{-3})	1×10^{10}	9×10^{10}	1×10^{10}

Table 11: Interface defect characteristics for the heterojunctions

Interface	Electron Capture Cross-Section (cm^2)	Hole Capture Cross-Section (cm^2)	Energy w.r.t Reference (eV)	Defect Density (cm^{-3})
CBTS /$CsSnCl_3$	$1x10^{-19}$	$1x10^{-19}$	0.6	$1x10^{10}$
$CsSnCl_3$ / ZnO	$1x10^{-19}$	$1x10^{-19}$	0.6	$1x10^{10}$

4 Conclusion

In conclusion, this study systematically optimised lead-free $CsSnCl_3$ solar cells with a *n-ip* heterostructure using SCAPS-1D for a diverse selection of potential electron transport layers (ETLs) and hole transport layers (HTLs). A range of heterostructures within the ITO/ETL/$CsSnCl_3$/HTL/Au architecture were assessed, and the most efficient module from 16 possible combinations with TiO_2, ZnO, C_{60}, and IGZO as ETLs and $CuSbS_2$, V_2O_5, CFTS, and CBTS as HTLs was optimised to identify structures yielding the highest performance. This study demonstrates the remarkable potential of lead-free $CsSnCl_3$ perovskite as an absorber layer for high-efficiency PSCs. Optimisation of the PSC heterostructure using SCAPS-1D numerical simulation software revealed that the combination of ZnO as the electron transport layer and CBTS as the hole transport layer resulted in the highest PCE of 16.95%. Furthermore, the influence of carrier density, defect density, and thickness of each layer on the overall module performance was evaluated. The results showcased that absorber defect density and acceptor density had no notable impact on PV efficiency, while absorber thickness had a significant impact on all 52 simulated modules of the chosen heterostructure. The initial device structure ITO/ZnO/$CsSnCl_3$/CBTS/Au yielded an efficiency of 7.15%. Optimisations led to an increase in efficiency 16.95% with a V_{oc} of 0.8 V, J_{sc} of 25.55 mA/cm^2, and FF of 82.89%. Additionally, this study establishes transferable design principles and guidelines for module fabrication, emphasizing the key role played by the defect density in HTL in limiting the performance, the indifference of the ETL, and the crucial role of absorber thickness. These findings provide a generalized framework for optimizing future

lead-free perovskite solar cells beyond the specific ZnO/CBTS configuration.

Conflict of Interest:

There is no conflict to declare.

References

[1] JOHN BONGAARTS. "IPCC, 2023: Climate Change 2023: Synthesis Report. IPCC, 184 p., doi: https://doi.org/10.59327/IPCC/AR6-9789291691647". In: *Population and Development Review* 50.2 (May 2024), pp. 577–580. issn: 1728-4457. doi: http://dx.doi.org/10.1111/padr.12632.

[2] Md Helal Miah et al. "Band gap tuning of perovskite solar cells for enhancing the efficiency and stability: issues and prospects". *RSC Adv.* 14.23 (May 2024), pp. 15876–15906.

[3] Yu Zhang, Huan-Ping Zhou, and College of Engineering, Peking University, Beijing 100871, China. "Intrinsic stability of organic-inorganic hybrid perovskite". *Wuli Xuebao* 68.15 (2019), p. 158804.

[4] Minhee Kim and Jinhyun Kim. "Recent research trends in inorganic charge transport materials for next-generation perovskite solar cells". *Renew. Sustain. Energy Rev.* 219.115835 (Sept. 2025), p. 115835.

[5] Saikumar Nair and Jignasa V Gohel. "A study on optoelectronic performance of perovskite solar cell under different stress testing conditions". Opt. Mater. (Amst.) 109.110377 (Nov. 2020), p. 110377.

[6] Zhiguo Zhang et al. "The importance of elemental lead to perovskites photovoltaics". *Chemistry of Inorganic Materials* 1.100017 (Dec. 2023), p. 100017.

[7] Okba Saidani, Abderrahim Yousfi, and Girija Shankar Sahoo. "Numerical investigation of $CsSnCI_3$ perovskite solar cells utilizing WS_2 and $CuSbS_2$ transport layers for enhanced efficiency beyond 24%". *Phys. Status Solidi (A)* 222.13 (July 2025).

[8] Teneng Assah Mbanga et al. "Charge carrier mobility and the recombination processes within a bulk heterojunction organic solar cell exhibiting disordered hopping". *J. Ren. Energies* 272 (Dec. 2024).

[9] Eli Danladi et al. "20.730% highly efficient lead-free $CsSnI_3$-based perovskite solar cells with various charge transport materials: a SCAPS-1D study". Multiscale Multidiscip. *Model. Exp. Des.* 8.1 (Jan. 2025).

[10] George G Njema, Joshua K Kibet, and Silas M Ngari. "A review of interface engineering characteristics for high performance perovskite solar cells". *Measurement: Energy* 2.100005 (June 2024), p. 100005.

[11] Thibault Lemercier et al. "A comparison of the structure and properties of opaque and semi-transparent NIP/PIN-type scalable perovskite solar cells". *Energies* 13.15 (July 2020), p. 3794.

[12] Zhiguo Zhang et al. "The importance of elemental lead to perovskites photovoltaics". *Chemistry of Inorganic Materials* 1.100017 (Dec. 2023), p. 100017.

[13] Okba Saidani, Abderrahim Yousfi, and Girija Shankar Sahoo. "Numerical investigation of $CsSnCI_3$ perovskite solar cells utilizing WS_2 and $CuSbS_2$ transport layers for enhanced efficiency beyond 24%". *Phys. Status Solidi (A)* 222.13 (July 2025)

[14] Teneng Assah Mbanga et al. "Charge carrier mobility and the recombination processes within a bulk heterojunction organic solar cell exhibiting disordered hopping". J. Ren. Energies 27.2 (Dec. 2024).